Modeling the Electrophoresis of Rigid Polyions: Application to Lysozyme

S. A. Allison and V. T. Tran
Department of Chemistry, Georgia State University, Atlanta, Georgia 30303 USA

ABSTRACT An algorithm is developed to determine the electrophoretic mobility of a rigid polyion modeled as a low dielectric volume element of arbitrary shape containing an arbitrary charge distribution. The solvent is modeled as a high dielectric continuum with salt distributed according to the linearized Poisson Boltzmann equation. Account is also taken of a Stern layer that separates the molecular surface and the surface of hydrodynamic shear, or Stern surface. Relaxation of the ion atmosphere because of the presence of the external field is ignored. The electrostatic and hydrodynamic problems are both solved by boundary element methods. The procedure is first applied to spherical polyions containing monopolar, dipolar, and quadrupolar charge distributions, and calculated mobilities are found to be in excellent agreement with the theory of Yoon and Kim. It is then applied to lysozyme by using models that account for the detailed shape and charge distribution of the enzyme. For reasonable choices of the molecular and Stern surfaces, calculated and experimental mobilities are found to be in fair agreement with each other. However, if a pH independent Stern layer (or, equivalently, translational diffusion constant, D_t) is assumed, the calculated mobilities exhibit a stronger pH dependence than is observed experimentally. A small increase in D_t with increasing pH could correct this discrepancy.

INTRODUCTION

Electrophoresis has proved to be an invaluable technique in the separation and characterization of polyions and colloids. The original electrophoresis experiments were carried out free in solution; hence the term "free solution electrophoresis." Because of convection problems caused by sample heating or vibration, these were difficult experiments to do and have largely been superseded by gel electrophoresis. Although gel electrophoresis has many advantages over the free solution method, it is more difficult to make contact with molecular models. One approach to determining free solution mobilities is to construct the Ferguson plot of mobility versus gel concentration (Holmes and Stellwagen, 1991) and extrapolate to zero gel concentration. Since the mid 1980's, capillary electrophoresis has emerged as a powerful technique (Grossman, 1992) and can be carried out free in solution or in a gel support medium. Because of the small linear dimensions of the capillary tube, convection problems associated with the traditional free solution experiments are largely eliminated. To date, determination of free solution mobilities by the capillary method have been restricted to smaller ions because of complications such as electroendoosmosis and the sticking of ions to the capillary walls. However, the technology of the method is in its infancy, and it is likely that these problems will be overcome. In view of these considerations coupled with recent developments in modeling the electrostatics and hydrodynamics of complex model systems, now is an opportune time to reexamine the theory of free solution electrophoresis.

Received for publication 10 January 1995 and in final form 17 February 1995.

Address reprint requests to Dr. Stuart A. Allison, Department of Chemistry, Georgia State University; University Plaza, Atlanta, GA 30303. Tel.: 404-651-1986; Fax: 404-651-3099; E-mail: chesa@gsusgil.gsu.edu.

0006-3495/95/06/2261/10 $2.00

The theory of electrophoresis (see, for example, Hunter, 1987) dates from the pioneering works on thin (Smoluchowski, 1921) and thick (Hückel, 1924) double layers. It was Henry (1931) who first provided a theory for the electrophoresis of spherical polyions valid for double layers of arbitrary thickness. In the Henry model, however, the charge distribution within the sphere is assumed to be spherically symmetric, and ion relaxation is ignored. Ion relaxation refers to the distortion of the ion atmosphere as a result of the action of the external electric field present. A number of investigators (Overbeek, 1950; Booth, 1950; Wiersema et al., 1966; O'Brien and White, 1978) have studied the effect of ion relaxation on the electrophoretic mobility of spheres containing a centrosymmetric charge distribution. In general, whether ion relaxation is important in this case depends on the polyion charge (or equivalently the electrostatic or "zeta" potential on the polyion surface), the polyion size, the salt concentration and the valency of its constituent ions, and the mobility of the ions. Under most conditions, however, the polyion charge is the most important factor. For a highly charged polyion such as DNA, ion relaxation is likely to be important (Schellman and Stigter, 1977), but for most proteins that contain low net charges it may be unimportant. Consider a "protein" modeled as a 2-nm-radius sphere at a monovalent salt concentration of 0.1 M at 20°C containing a central charge of $\pm 18.85q$ (where q is the protonic charge). Ionic relaxation reduces the electrophoretic mobility of this model protein by only 10%, and the effect decreases as the magnitude of the net charge decreases. Inasmuch as most proteins have net charges lower than this, ignoring relaxation is likely to be an entirely reasonable approximation. Unlike in the Henry model, however, proteins are not spherical and their charge distributions are complex. The problem of an arbitrary charge distribution in a spherical polyion without ion relaxation was considered recently by Yoon (1991). The additional approximation was made in this work that the ion

atmosphere is distributed according to the linearized Poisson-Boltzmann (PB) equation. Because the validity of the linearized PB equation and the neglect of ion relaxation are directly correlated with net polyion charge, these two approximations are complementary. In addition to spherical polyions, the electrophoresis of long cylinders has been treated without (Henry, 1931) and with ion relaxation (Stigter, 1978). Yoon and Kim (1989) have determined the electrophoretic mobility of prolate and oblate ellipsoids at low uniform surface potential, where ion relaxation is ignored and the linear PB equation describes the potential.

The objective of this work is to develop a method of determining the electrophoretic mobility of rigid model polyions of arbitrary shape and charge distribution. The polyion is represented as a low dielectric volume element enclosed by a "molecular surface" with dielectric constant ϵ_i impermeable to penetration by solvent and mobile ions. Outside the molecular surface is the solvent characterized as a continuum with uniform dielectric constant ϵ_o. The mobile ions in the solvent are distributed according to the linearized PB equation. Ion relaxation will be ignored and it will be assumed that the external field is low enough that orientation of the polyion by the electric field has no significant effect on the polyion's mobility. Following the nomenclature of colloid science (see, for example, Hunter, 1987, or Shaw, 1980), it is also convenient to define a Stern surface that entirely encloses the molecular surface. Between the two surfaces lies the Stern layer, which contains solvent and mobile ions that move with the polyion as a rigid body. In the next section, the procedure used to compute the electrophoretic mobility is described. Briefly, what is required is a numerical solution of the linearized PB equation to obtain the electrostatic potential by using the molecular surface and a numerical solution of the Navier-Stokes equation by using the Stern surface. Boundary element methods are used in both cases. The procedure is then applied to some simple model problems to verify the method, and finally to detailed models of lysozyme based of the detailed charge distribution and surface topography of the enzyme.

COMPUTATIONAL STRATEGY

To understand how an electrophoretic mobility is obtained from a modeling study, it will be useful to follow the O'Brien and White (1978) strategy of considering two distinct transport cases. In the transport 1 (T1) case, no external electric field $\mathbf{e}$ is present, and the single polyion is translated with velocity $\mathbf{u}$ and rotated with angular velocity $\boldsymbol{\omega}$ in an unbounded fluid. Except for the disturbance produced by the polyion itself, the fluid is stationary. The total force, $\mathbf{z}(1)$, and torque, $\mathbf{t}(1)$, are related to $\mathbf{u}$ and $\boldsymbol{\omega}$ by (Brenner, 1963; Kim and Karrila, 1991)

$$\mathbf{z}(1) = -\eta \mathbf{K} \cdot \mathbf{u} - \eta \boldsymbol{M}^{\mathrm{T}} \cdot \boldsymbol{\omega}, \tag{1}$$

$$\mathbf{t}(1) = -\eta \mathbf{M} \cdot \mathbf{u} - \eta \boldsymbol{P} \cdot \boldsymbol{\omega}, \tag{2}$$

where η is the solvent viscosity, $\boldsymbol{K}$ and $\boldsymbol{P}$ are the translational and rotational friction tensors, and $\boldsymbol{M}$ is a coupling tensor. Superscript T denotes the transpose. The forces and torques are computed as described below and the components of $\boldsymbol{K}$, $\boldsymbol{M}$, and $\boldsymbol{P}$ are readily obtained by translating or rotating the model polyion along or about a single axis. This is the same strategy used to derive the orientationally averaged translational (D_t) and rotational (D_r) diffusion constants of model polyions (Brune and Kim, 1993):

$$D_t = \frac{k_B T}{3\eta} \mathrm{Tr}[\boldsymbol{K}'], \tag{3}$$

$$D_r = \frac{k_B T}{3\eta} \mathrm{Tr}[\boldsymbol{P}'], \tag{4}$$

where Tr denotes the trace and mobility tensors $\boldsymbol{K}'$ and $\boldsymbol{P}'$ are related to $\boldsymbol{K}$, $\boldsymbol{M}$, and $\boldsymbol{P}$ by

$$\boldsymbol{K}' = (\boldsymbol{K} - \boldsymbol{M}^{\mathrm{T}} \cdot \boldsymbol{P}^{-1} \cdot \boldsymbol{M})^{-1}, \tag{5}$$

$$\boldsymbol{P}' = (\boldsymbol{P} - \boldsymbol{M} \cdot \boldsymbol{K}^{-1} \cdot \boldsymbol{M}^{\mathrm{T}})^{-1}, \tag{6}$$

where the superscript -1 represents an inverse.

In the transport 2 (T2) case, the polyion is held stationary in constant external electric field $\mathbf{e}$ in an unbounded fluid. As before, the fluid is stationary except for the disturbance produced by the external field in the vicinity of the polyion itself. The total force $\mathbf{z}(2)$ and torque $\mathbf{t}(2)$ are related to $\mathbf{e}$ by

$$\mathbf{z}(2) = \eta \boldsymbol{Q} \cdot \mathbf{e}, \tag{7}$$

$$\mathbf{t}(2) = \eta \mathbf{R} \cdot \mathbf{e}. \tag{8}$$

As in the T1 case, the components of $\boldsymbol{Q}$ and $\boldsymbol{R}$ are readily obtained from the force and torque components when the external field is applied along particular directions.

Now consider a polyion in a particular orientation that is translating under steady-state conditions with velocity $\mathbf{u}$ in an external field $\mathbf{e}$. This can be viewed as a superposition of the T1 and T2 cases with a net force of zero. Solving for $\mathbf{u}$ yields

$$\mathbf{u} = (\boldsymbol{K}^{-1} \cdot \boldsymbol{Q}) \cdot \mathbf{e}. \tag{9}$$

Provided that $\mathbf{e}$ is sufficiently small that the orientation of the polyion is negligible, we can average Eq. 9 over all possible orientations, which leads directly to the electrophoretic mobility μ:

$$\mu = \frac{u}{e} = \frac{1}{3}\mathrm{Tr}[\boldsymbol{K}^{-1} \cdot \boldsymbol{Q}]. \tag{10}$$

To determine the mobility, one must first determine $\boldsymbol{K}$ and $\boldsymbol{Q}$, which requires calculation of the total force on the polyion.

The total force can be written as a sum of hydrodynamic, $\mathbf{z}_h$, and electrostatic, $\mathbf{z}_e$, components (Allison and Nambi, 1992, 1994):

$$\mathbf{z} = \mathbf{z}_h + \mathbf{z}_e, \tag{11}$$

where

$$\mathbf{z}_h = -\int_S \mathbf{h}(\mathbf{y})dS_y \approx -\sum_j \mathbf{h}_j A_j, \quad (12)$$

$$\mathbf{z}_e = -\int_V \mathbf{s}(\mathbf{y})dV_y \approx -\sum_k \mathbf{s}_k V_k. \quad (13)$$

In relation 12 the surface stress forces per unit area, $\mathbf{h}(\mathbf{y})$, are integrated over the surface of the polyion. The polyion surface is broken up into N planar triangular surfaces, and the assumption is made that $\mathbf{h}$ is uniform over each triangular surface. The values of $\mathbf{h}_j$ are obtained by solving the Navier–Stokes equation by the boundary integral equation method discussed below. In relation 13, $\mathbf{s}(\mathbf{y})$ is the external force per unit volume on the fluid, and the volume integral extends over the fluid surrounding the polyion. Similar to the hydrodynamic force, the volume is broken up into discrete elements, and $\mathbf{s}$ is assumed to be uniform within each element. The corresponding quantities for the total torques on the polyion are obtained by replacing $\mathbf{h}$ and $\mathbf{s}$ under the integrals in relations 12 and 13 with $\mathbf{y} \times \mathbf{h}$ and $\mathbf{y} \times \mathbf{s}$, respectively.

The external force $\mathbf{s}$ is related to the electrostatic potential ϕ and the charge density ρ by

$$\mathbf{s}(\mathbf{y}) = -\rho(\mathbf{y}) \nabla\phi(\mathbf{y}). \quad (14)$$

It will prove convenient to write ϕ as the sum of the electrostatic potential that is due to the polyion itself in the absence of an external field, ϕ_0, and that which is due to the external field, ϕ_e. Because ion relaxation is ignored in this work, the charge density is just the equilibrium charge distribution ρ_0, which is related to ϕ_0 by the Boltzmann distribution. Thus we can write

$$\mathbf{s}(\mathbf{y}) = -\rho_0(\mathbf{y})[\nabla\phi_0(\mathbf{y}) + \nabla\phi_e(\mathbf{y})] = \mathbf{s}_0(\mathbf{y}) + \mathbf{s}_e(\mathbf{y}). \quad (15)$$

In the absence of an external field, $\mathbf{z}_e(1)$ must vanish, which shows that $\mathbf{s}_0$ makes no net contribution to transport in either the case 1 or the case 2 situation. As calculating translational or rotational diffusion constants involve only the T1 case and as $\mathbf{s}_e$ vanishes in this situation, external forces do not contribute to these transport properties. In the T2 case, however, $\mathbf{s}_e$ produces a nonvanishing $\mathbf{z}_e(2)$, and these external forces have to be accounted for.

It is possible to solve for the total forces in terms of the transport of the corresponding uncharged polyion by using the Teubner (1982) relation given by Eq. 16,

$$z_{hj} = \mathbf{u} \cdot \mathbf{z}_{h0}^{(j)} + \int_V \mathbf{v}^{(j)}(\mathbf{y}) \cdot \mathbf{s}(\mathbf{y})dV_y, \quad (16)$$

where z_{hj} is the jth component of the hydrodynamic force on the polyion, $\mathbf{v}^{(j)}(\mathbf{y})$ is the fluid velocity at $\mathbf{y}$ that is due to translation of the equivalent uncharged polyion translating with unit velocity in the j direction, and $\mathbf{z}_{h0}^{(j)}$ is the hydrodynamic force on the uncharged polyion translating with unit velocity along j.

In the T1 case, the jth component of the total force is simply

$$z_j(1) = \mathbf{u} \cdot \mathbf{z}_{h0}^{(j)}. \quad (17)$$

In the T2 case, it is straightforward to show that

$$z_j(2) = \int_V [\mathbf{v}^{(j)}(\mathbf{y}) - \mathbf{i}_j] \cdot \mathbf{s}_e(\mathbf{y})dV_y, \quad (18)$$

where $\mathbf{i}_j$ is the unit vector in the j direction.

BOUNDARY ELEMENT METHODS FOR ELECTROSTATICS AND HYDRODYNAMICS

For both electrostatic and hydrodynamic calculations, boundary element (BE) methods are particularly convenient in the present application. As discussed above, the polyion surface is subdivided into N triangular platelets, as illustrated in Fig. 1. How these structures are generated is discussed below. In addition to the constancy of the hydrodynamic stress force over any platelet, it is further assumed that the electrostatic potential and its normal derivative are constant as well. The electrostatic problem will be considered first. Because the BE approach to electrostatics is well described elsewhere (Yoon and Lenhoff, 1990; Juffer et al., 1991; Zhou, 1993), the following discussion will be kept brief.

The polyion is assumed to be rigid and to have an arbitrary shape as depicted in Fig. 1. The interior of the polyion contains an arbitrary charge distribution and a uniform dielectric

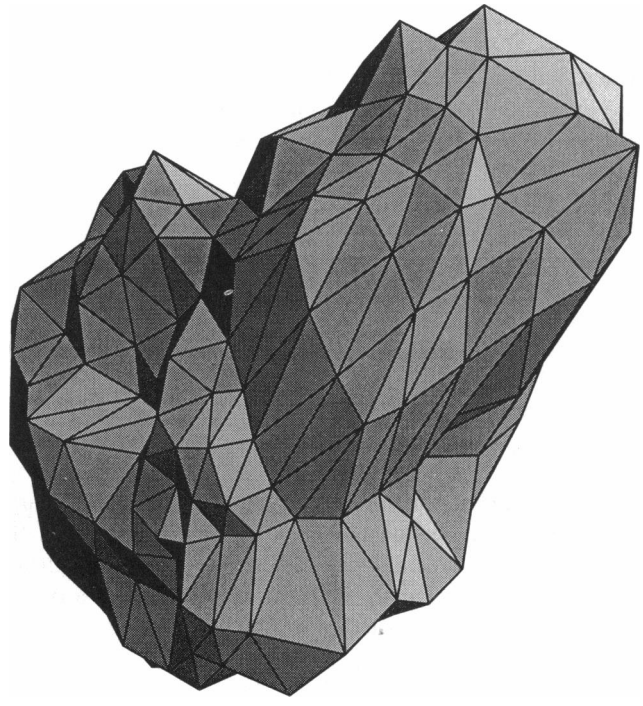

FIGURE 1 Model surface for lysozyme. The enzyme is represented as 512 triangular plates derived from the crystal structure. The assumption is made that electrostatic potentials, the normal derivative of the electrostatic potential, and hydrodynamic stress forces are constant over the surface of each platelet.

constant ϵ_i. The interior is assumed to be impermeable to penetration by salt and mobile ions. The surrounding fluid has uniform dielectric constant ϵ_o, and the mobile ions are distributed according to the linearized PB equation. Under these conditions, it is possible to express the electrostatic potential anywhere in space given the charge distribution, the surface topography, and electrostatic potential and its normal derivative over the polyion surface (Yoon and Lenhoff, 1990; Juffer et al., 1991; Zhou, 1993). For our purposes, it is convenient to divide the electrostatic problem into the calculation of ϕ_0 (electrostatic potential in the absence of the external electric field) and ϕ_e (electrostatic potential due to the external field) separately. Following the notation of Zhou (1993), let $\mathbf{f}_0$ denote the $1 \times N$ column vector where the components represent ϕ_0 on a particular platelet. Similarly, let $\mathbf{g}_0$ denote a $1 \times N$ column vector with

$$(g_0)_j = \epsilon_i \left(\frac{\partial \phi_0}{\partial n}\right)_{\text{inside}} = \epsilon_o \left(\frac{\partial \phi_0}{\partial n}\right)_{\text{outside}}, \tag{19}$$

where the derivatives are outward normal derivatives taken in the limit of a field point approaching the surface from the interior or exterior of the polyion. Let $\mathbf{y}_j$ denote a reference position vector on platelet j. Making use of Green's second identity and the singular solutions of the Poisson and linearized PB equations, it can be shown (Zhou, 1993) that

$$\begin{aligned} \frac{1}{2}\mathbf{f}_0 &= \frac{1}{\epsilon_i}\mathbf{v} + \boldsymbol{A}\cdot\mathbf{f}_0 + \frac{1}{\epsilon_i}\boldsymbol{C}\cdot\mathbf{g}_0, \\ -\frac{1}{2}\mathbf{f}_0 &= \boldsymbol{B}\cdot\mathbf{f}_0 + \frac{1}{\epsilon_o}\boldsymbol{D}\cdot\mathbf{g}_0, \end{aligned} \tag{20}$$

where $\mathbf{v}$ is a $1 \times N$ column vector of vacuum potentials that are due to the array of point charges distributed inside the polyion and $\boldsymbol{A}$, $\boldsymbol{B}$, $\boldsymbol{C}$, and $\boldsymbol{D}$ are $N \times N$ matrices:

$$\begin{aligned} v_j &= \sum_{k=1}^{p} \frac{q_k}{|y_j - r_k|}, \\ A_{jk} &= I_1(y_j, k, 0), \\ B_{jk} &= I_1(y_j, k, \kappa), \\ C_{jk} &= I_2(y_j, k, 0), \\ D_{jk} &= I_2(y_j, k, \kappa). \end{aligned} \tag{21}$$

Above, p is the number of polyion charges and the kth charge of magnitude q_k is located at position $\mathbf{r}_k$. Also, κ is the Debye–Huckel screening parameter and I_1 and I_2 are surface integrals over particular platelets. Let $\mathbf{y}$ be some arbitrary field point and S_k the surface of platelet k. Then

$$\begin{aligned} I_1(\mathbf{y}, k, \kappa) &= \int_{S_k} \frac{(1+\kappa x)e^{-\kappa x}}{4\pi x^3}\mathbf{n}'\cdot\mathbf{x}\,dS', \\ I_2(\mathbf{y}, k, \kappa) &= \int_{S_k} \frac{e^{-\kappa x}}{4\pi x}\,dS', \end{aligned} \tag{22}$$

where $\mathbf{x} = \mathbf{y}' - \mathbf{y}$, $\mathbf{y}'$ is some surface point, $\mathbf{x} = |\mathbf{x}|$, and $\mathbf{n}'$ is the surface unit normal at $\mathbf{y}'$ pointing outward from the polyion surface into the solvent. In this work, I_1 and I_2 are solved by an iterative method in which the platelets are broken up into a mesh of smaller triangles and the integral approximated by a discrete sum over the integrand evaluated at the center of the smaller triangles. The surface is broken up into successively finer meshes until the approximate integral converges to within a predefined tolerance level ($|1 - I_{old}/I_{new}| \leq 10^{-3}$ in this work).

Equation 20 can be formulated as a $2N \times 2N$ matrix problem that can be inverted to yield $\mathbf{f}_0$ and $\mathbf{g}_0$. The potential ϕ_0 at any field point $\mathbf{y}$ in the solvent region is given by

$$\phi_0(\mathbf{y}) = -\sum_{k=1}^{N}\left[\frac{g_{0k}}{\epsilon_o}I_2(\mathbf{y}, k, \kappa) + f_{0k}I_1(\mathbf{y}, k, \kappa)\right]. \tag{23}$$

The charge density at the level of the linear PB equation is $-2q^2n_0\phi_0(\mathbf{y})/k_BT$, where $q = 4.8 \times 10^{-10}$ esu, n_0 is the monovalent salt concentration far from the polyion, and k_BT is Boltzmann's constant times absolute temperature.

The electrostatic potential that is due to the external field, $\phi_e(\mathbf{y})$, must be handled slightly differently because it does not vanish far from the polyion. This part of the problem involves solving for the electrostatic potential around the low dielectric polyion in the absence of fixed and mobile charges subject to the boundary condition $\phi_e(\mathbf{y}) = -\mathbf{e}\cdot\mathbf{y}$ as $|\mathbf{y}|$ goes to infinity. Using the terminology of Eqs. 20 but letting $\mathbf{f}_e$ and $\mathbf{g}_e$ refer to the $1 \times N$ column vectors of the external field problem, it can be shown that

$$\begin{aligned} \frac{1}{2}\mathbf{f}_e &= \boldsymbol{A}\cdot\mathbf{f}_e + \frac{1}{\epsilon_i}\boldsymbol{C}\cdot\mathbf{g}_e, \\ -\frac{1}{2}\mathbf{f}_e + \mathbf{f}_u &= \boldsymbol{A}\cdot\mathbf{f}_e + \frac{1}{\epsilon_o}\boldsymbol{C}\cdot\mathbf{g}_e, \end{aligned} \tag{24}$$

where $f_{uj} = -\mathbf{y}_j\cdot\mathbf{e}$ represents the electrostatic potential at $\mathbf{y}_j$ in the absence of a dielectric discontinuity at the polyion surface. The matrices $\boldsymbol{A}$ and $\boldsymbol{C}$ are the same as before, and it is straightforward to invert a $2N \times 2N$ matrix and obtain $\mathbf{f}_e$ and $\mathbf{g}_e$. To calculate the external force $\mathbf{s}_e(\mathbf{y})$ given by Eq. 15 we actually need the gradient of ϕ_e evaluated in the solvent region. This is given by

$$\nabla_y\phi_e(\mathbf{y}) = -\mathbf{e} - \sum_{k=1}^{N}\left[\frac{g_{ek}}{\epsilon_o}\mathbf{H}_2(\mathbf{y}, k) + f_{ek}\mathbf{H}_1(\mathbf{y}, k)\right], \tag{25}$$

where

$$\begin{aligned} \mathbf{H}_2(\mathbf{y}, k) &= \int_{S_k} \frac{\mathbf{x}}{4\pi x^3}\,dS', \\ H_1(y, k) &= \int_{S_k} \frac{1}{4\pi x^5}[3(\mathbf{n}'\cdot\mathbf{x})\mathbf{x} - x^2\mathbf{n}']dS' \end{aligned} \tag{26}$$

and $\mathbf{x} = \mathbf{y}' - \mathbf{y}$ (see Eqs. 22). The surface integrals $\mathbf{H}_1$ and $\mathbf{H}_2$ are evaluated in the same iterative matter that is used to evaluate I_1 and I_2. Some care must be taken when $\mathbf{y}$ is very close to some particular platelet (call it k') on the molecular surface. It is straightforward to show that the term in brackets on the right-hand side of Eq. 25 that is due to k' has a leading component that is normal to the k' surface. In this situation the approximation is made:

$$\nabla_y \phi_e(\mathbf{y}) = [\nabla_y \phi_e(\mathbf{y})]' + \mathbf{n}_k \left[\frac{g_{ek}}{\epsilon_o} - \mathbf{n}_k \cdot [\nabla_y \phi_e(\mathbf{y})]' \right], \quad (27)$$

where $[\nabla \phi_e(\mathbf{y})]'$ represents the contribution of Eq. 25 of all terms excluding the $k = k'$ term.

The hydrodynamic problem is solved in a matter entirely analogous to the solution of the electrostatic problem (Ladyzhenskaya, 1963; Youngren and Acrivos, 1975; Kim and Karrila, 1991; Allison and Nambi, 1992). Use is made of the singular solution of the Navier–Stokes equation coupled with Green's theorem. Given a rigid polyion translating with velocity $\mathbf{v}(\mathbf{y}') = \mathbf{u} + \boldsymbol{\omega} \times \mathbf{y}'$ ($\mathbf{u}$ and $\boldsymbol{\omega}$ are constant translational and rotational velocity vectors and $\mathbf{y}'$ is some point on the polyion surface) through an incompressible liquid that is at rest far from the polyion, it can be shown that the fluid velocity at $\mathbf{y}$ is

$$\mathbf{v}(\mathbf{y}) = -\int_S \boldsymbol{U}(\mathbf{x}, \mathbf{y}) \cdot \mathbf{h}(\mathbf{x}) dS_x - \int_V \boldsymbol{U}(\mathbf{x}, \mathbf{y}) \cdot \mathbf{s}(\mathbf{x}) dV_x, \quad (28)$$

where S and V refer to the polyion surface and surrounding fluid, respectively, $\mathbf{h}$ and $\mathbf{s}$ are the surface stress and external forces, and (given $\mathbf{r} = \mathbf{y} - \mathbf{x}$, $r = |\mathbf{r}|$)

$$\boldsymbol{U}(\mathbf{x}, \mathbf{y}) = \frac{1}{8\pi\eta r}[\boldsymbol{I} + \boldsymbol{R}(\mathbf{x}, \mathbf{y})], (\mathbf{R}(\mathbf{x}, \mathbf{y}))_{ij} = \frac{r_i r_j}{r^2}. \quad (29)$$

In Eq. 29, η is the solvent viscosity and $\boldsymbol{I}$ is the 3×3 identity matrix. Breaking up the surface into N platelets and the surrounding volume into M volume elements yields for Eq. 28

$$\mathbf{v}(\mathbf{y}) = \sum_{j=1}^{N} \boldsymbol{E}_j(\mathbf{y}) \cdot \mathbf{h}_j + \sum_{k=1}^{M} \boldsymbol{G}_k(\mathbf{y}) \cdot \mathbf{s}_k, \quad (30)$$

where $\boldsymbol{E}_j$ and $\boldsymbol{G}_k$ are surface and volume integrals of $\mathbf{U}$ over elements j and k, respectively. At the polyion surface ($\mathbf{y} = \mathbf{y}'$), we know $\mathbf{v}(\mathbf{y})$ from the stick boundary conditions. Inasmuch as $\mathbf{s}_k$ is known from prior solution of the electrostatic problem, the only unknowns in Eq. 30 are the values of $\mathbf{h}_j$, and these can be solved by Gauss–Seidel iteration (Allison and Nambi, 1992). In general, the surface used in the electrostatic calculation (molecular surface) is different from that used in hydrodynamics (Stern layer). This point will be discussed in the application to lysozyme.

TEST CASES: SPHERICAL POLYIONS

Once the polyion is defined, external forces and stress forces are computed following the procedures of the previous section. Then, following the section on Computational Strategy, the total forces on the polyion, the $\boldsymbol{K}$ and $\boldsymbol{Q}$ tensors, and finally the electrophoretic mobility are determined. As a first test case, consider a spherical polyion of radius $a = 2.03$ nm with a net charge of $12.8q$ (q is the protonic charge) at a monovalent salt concentration of 0.15 M at 0°C. The interior/exterior dielectric constants are taken to be 2 and 78, respectively. In the numerical study, the tesselation procedure of Pakdel and Kim (1989) is used to represent the sphere as a geodesic surface of 128 triangular platelets as shown in Fig. 2. The distance from the origin to the center of each platelet is about 2.03 nm. From T1 transport calculations using this structure, D_t and D_r agree with the known analytical values to within 1%. An electrophoretic mobility of 8.95×10^{-5} cm^2/V s is obtained from the BE numerical procedure, which is in excellent agreement with the analytical value of 8.91×10^{-5} cm^2/V s predicted by Henry's (1931) equations. A more stringent test of the electrostatic model is a spherical polyion containing a pure dipole. The sphere is centered at the origin, and charges of $-12.8q$ and $+12.8q$ are placed at positions (in nanometers) (−1.53, 0, 0) and (+1.53, 0, 0) respectively. The BE mobility turns out to be approximately a factor of 10^3 times smaller than for the monopole charge case considered previously; in other words, it is negligible. This is consistent with the theory of Yoon (1991), which predicts that only the monopole and quadrupole moments contribute to the electrophoretic mobility. Furthermore, the Yoon theory predicts that the contribution of the quadrupole moment vanishes when an isotropic average over all possible orientations is taken. As a third test case, consider a sphere with a quadru-

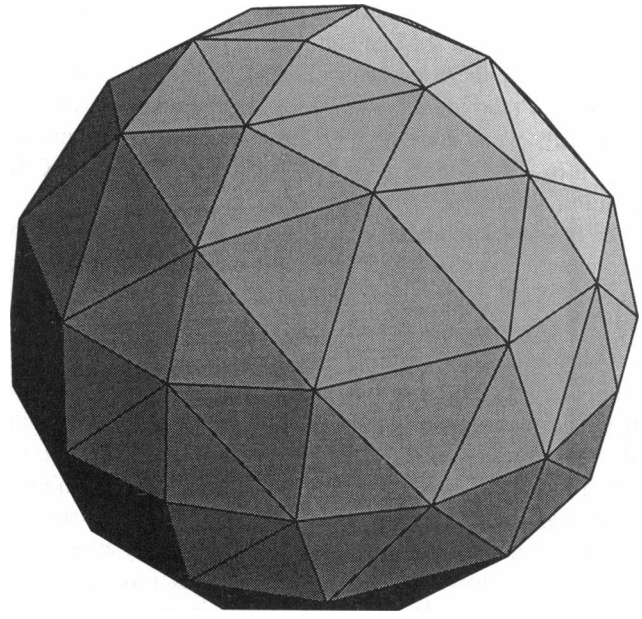

FIGURE 2 Model sphere for test cases. The spherical polyion is represented as 128 triangular plates.

polar charge distribution with charges $-6.4q$, $+12.8q$, and $-6.4q$ placed at (−1.53, 0, 0), (0, 0, 0), and (+1.53, 0, 0), respectively. The BE procedure and the theory of Yoon yield $\mu = 2.016 \times 10^{-5}$ and 2.045×10^{-5} cm^2/V s, respectively, for translation in the x direction. Also, the BE procedure gives $(\mu)_{y \text{ or } z} \approx -0.5(\mu)_x$, as predicted by Yoon. For spherical polyions, the BE method is yielding correct mobilities.

LYSOZYME

Hen eggwhite lysozyme is an excellent enzyme for modeling purposes because it has been so thoroughly studied. It consists of 129 amino acid residues and has a molecular weight of 14,800 gm/mol. Diffusion constants (Dubin et al., 1967, 1971; Kuntz and Kauzmann, 1974; Squire and Himmel, 1979) and electrophoretic mobilities (Beychok and Warner, 1959) are available. In addition, the pK values of the charged residues are known (Kuramitsu and Hamaguchi, 1980), so the charge state of the enzyme can be predicted with considerable accuracy over a broad pH range. As lysozyme is known to dimerize above a pH of ~6 (Sophianopoulos and Van Holde, 1964), we shall concentrate on the mobility in the pH range 2–6.

The translational diffusion constant of lysozyme measured by light scattering varies from 10.6×10^{-7} (Dubin et al., 1971) and 11.3×10^{-7} cm^2/s (Dubin et al., 1967; Squire and Himmell, 1979) corrected to 20°C. A consensus value of 11.1×10^{-7} cm^2/s reported by Kuntz and Kauzmann (1974) falls within this range. Although D_t is reasonably well known, there is some uncertainty in its value. It is unclear whether some of this uncertainty could be due to differences in solution conditions (pH or salt). Because the value of 10.6×10^{-7} cm^2/s reported in the latter light scattering study (Dubin et al., 1971) were carried out under conditions (T = 20°C, 0.10 M salt, pH = 4) that were similar to those employed in the electrophoresis experiments of Beychok and Warner (1959) (T = 0°C, 0.15 M salt, pH = 1.5–5.9) this value of D_t along with the consensus value of 11.1×10^{-7} cm^2/s will be used in the modeling studies. As the electrophoresis experiments were done at 0°C, the diffusions constants are scaled by T/η, which reduces D_t from its value at 20°C by a multiplicative factor of 0.5214.

In the detailed model studies, account will be taken of the protein shape and charge distribution. To understand better how the surfaces depicted in Fig. 1 are generated, consider Fig. 3. Associated with each triangular platelet are three vertex vectors denoted by the dashed arrows that radiate outward from some convenient origin. In the case of lysozyme, we have the coordinates of the nonhydrogen atoms from the Brookhaven Protein Databank (61yz.brk), and the origin is taken to be the center of mass. Associate with each nonhydrogen atom an "exclusion radius" σ. In general, σ can vary from atom to atom, but in this study we shall assume a uniform value. How far out one has to go before the vertex vector no longer falls within any exclusion sphere defines the endpoint of the vertex vector. To begin, we start with six vertex vectors that produce a roughly octahedral surface consisting of eight platelets. This structure will be referred to as the starting octahedron. The midpoint of each edge of each platelet is then taken as the direction of a new vertex vector. The endpoint of the new vertex vector is found in the same manner as that of the original vectors. Basically, each of the original platelets is replaced by a mesh of four new ones that conform more accurately to the actual shape of the macromolecule. This simple mesh refinement procedure helps to prevent the formation of slender triangles with long edges that are unsuitable in BE methods (Brune and Kim, 1993). Proceeding along these lines, surfaces consisting of 8, 32, 128, 512, etc. platelets can be constructed. We shall restrict ourselves to 128 and 512 platelets in this work.

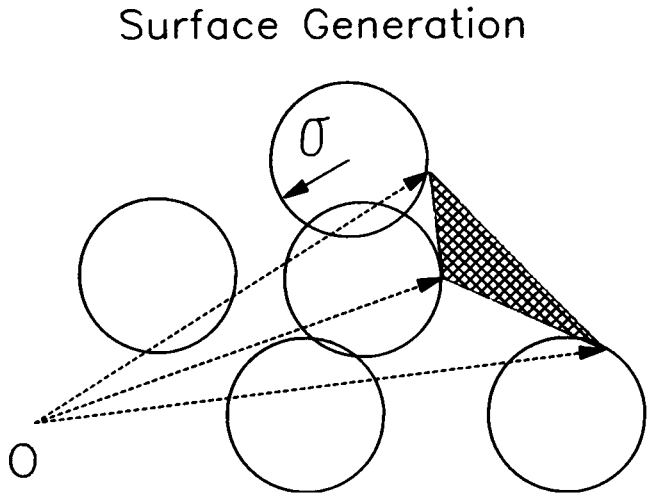

FIGURE 3 Schematic of the surface generation procedure. An exclusion radius σ is associated with each nonhydrogen atom of the crystal structure. Three vertex vectors (denoted by the dashed arrows) define a single platelet on the polyion surface.

The most straightforward way of defining the Stern surface is to determine which uniform exclusion radius σ_s produces a structure with the correct D_t. One starts with a trial σ_s and constructs the Stern surface. Then a T1 calculation is carried out to determine the resistance tensors, $\boldsymbol{K}$, $\boldsymbol{M}$, and $\boldsymbol{P}$ according to Eqs. 1 and 2. From Eqs. 3–6 it is straightforward to calculate D_t corresponding to this structure. Several iterations lead to a model structure with a σ_s that corresponds to D_t known experimentally.

Shown in Fig. 4 are experimental (filled squares), Henry (+), and BE detailed model (diamonds) mobilities plotted versus pH. A diffusion constant of 10.6×10^{-7} cm^2/s (20°C) is used to define the hydrodynamic radius used in the Henry model (a = 2.03 nm) and the exclusion radius in the BE models (N = 128, $\epsilon_i = 2$, $\epsilon_o = 78$, σ_s = 0.45 nm). From the pK values of Kuramitsu and Hamaguchi (1980), the total charge Q of lysozyme (in protonic units) is estimated to be 16.79, 13.96, 12.80, 10.23, and 8.98 at pH = 2, 3, 4, 5, 6, respectively. Fractional charges derived from these pK's are placed at the crystallographic coordinates of all charged residues in the BE model studies. It is clear from this figure that both the Henry model, which treats the polyion as a sphere with a centrosymmetric charge distribution, and the BE

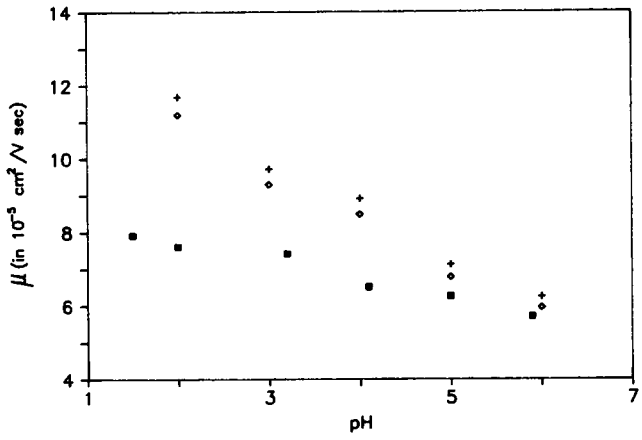

FIGURE 4 Henry and BE mobilities versus pH. Comparison of Henry (+) and BE (◇) models for $D_t(20°C) = 10.6 \times 10^{-7}$ cm²/s. In the BE model, $N = 128$ and no Stern layer is included. Experimental mobilities of Beychok and Warner (1959) are also shown (■).

model, which accounts more accurately for the shape and charge distribution, predict nearly the same electrophoretic mobility. The calculations substantially overestimate the mobility at low pH but approach the correct value at a pH of ~6. Similar results are shown in Fig. 5, except that a diffusion constant of 11.1×10^{-7} cm²/s (20°C) is used to define the hydrodynamic radius in the Henry model ($a = 1.93$ nm) and the exclusion radius in the BE models ($N = 128$, $\sigma_s = 0.39$ nm). The discrepancy between calculated and experimental mobilities is actually greater in Fig. 5.

In the cases represented in Figs. 4 and 5, no distinction has been made between the molecular surface and the Stern surface. As shown below, how one treats the Stern layer or, more precisely, the layer of solvent and mobile ions near the macromolecular surface, has a significant effect on calculated mobilities. Teller et al. (1979) and Venable and Pastor (1988) have carried out detailed bead model studies (Garcia de la Torre and Bloomfield (1981) of the diffusion constants of several proteins. They found that it is necessary to include a hydration shell of tightly bound solvent to get agreement between calculated and experimental diffusion constants. In the present work, a σ_s in the range of 0.35–0.48 nm is also consistent with a partial layer of bound waters because a value of ~0.30 nm (the sum of the van der Waal radii of a non-H protein atom plus water) is a more reasonable value for the exclusion radius σ corresponding to the actual molecular surface. It has been known for a long time that water in the immediate vicinity of a protein has properties that are very different from that of water free in solution. The reviews by Kuntz and Kauzmann (1974) and Rupley and Careri (1991) discuss this in depth. Specifically, NMR experiments on lysozyme (reviewed by Careri, 1991) show that surface waters are substantially less mobile than bulk waters. Molecular dynamics simulations on lysozyme (Brooks and Karplus, 1989) and bovine pancreatic trypsin inhibitor (Levitt and Sharon, 1988) confirm this. The molecular dynamics studies go on to show that waters near charged and apolar protein residues are less mobile than those near polar residues. In what follows, we shall model the fluid around lysozyme in terms of molecular and Stern surfaces with a Stern layer between. In this model, the assumption is made that the solvent and the ions within the Stern layer are immobile relative to the macromolecule. The NMR and molecular dynamics studies show that this Stern layer modeling approach is a simplification of the actual properties of the solvent and "mobile" ions near the protein surface. Nonetheless, it does account in an approximate way for the reduced mobility of the solvent/ions near the protein surface. Given the other assumptions of this work (rigid protein, two dielectric model, and use of the linearized PB equation to estimate electrostatic potentials and charge densities in the solvent and the Stern layer region), this seems entirely reasonable.

Fig. 6 shows experimental mobilities (squares) along with BE results ($N = 128$, $\sigma = 0.30$ nm). In the case of the diamonds, $\sigma_s = 0.39$ nm (which yields $D_t(20°C) = 11.1 \times 10^{-7}$ cm²/s), and in the case of the crosses; $\sigma_s = 0.45$ nm

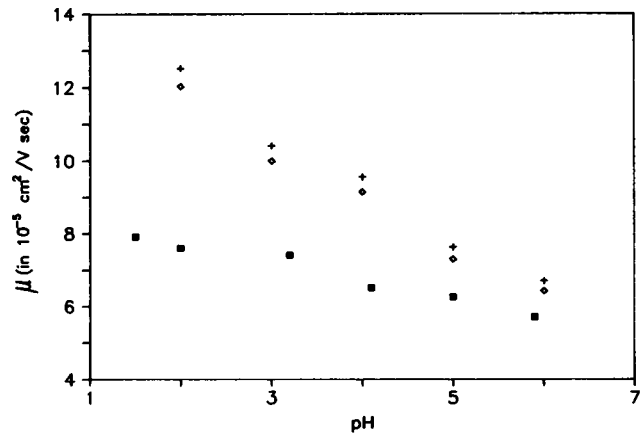

FIGURE 5 Henry and BE mobilities versus pH. Similar to Fig. 4, except that $D_t(20°C) = 11.1 \times 10^{-7}$ cm²/s.

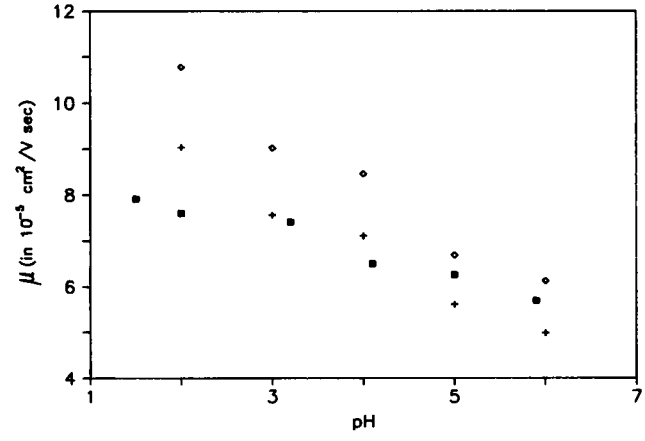

FIGURE 6 Experimental and BE mobilities (Stern layer included). ■, Experimental mobilities. For the BE results, ◇ and + correspond to values of σ_s chosen to give $D_t(20°C) = 11.1 \times 10^{-7}$ and 10.6×10^{-7} cm²/s, respectively. In the BE models; $N = 128$, $\epsilon_i = 2$, $\sigma = 0.30$ nm, and the 101 crystallographic waters have been included in generating the molecular and the Stern surfaces.

(which yields $D_t(20°C) = 10.6 \times 10^{-7}$ cm^2/s). Including a Stern layer reduces the calculated mobilities and brings them into better agreement with experiment. Holding other variables (including σ_s) constant and increasing the volume of the Stern layer by reducing σ reduces the absolute value of the mobility because the absolute value of the net polyion charge plus the charge contained in the Stern layer is lower than the absolute value of the net polyion charge itself. Except at pH = 2, the calculated and experimental mobilities are seen to be in fair agreement with each other for physically reasonable choices of σ and σ_s. In Fig. 6 the 101 waters present in the crystal structure have been included in calculating both the Stern and molecular surfaces. Including these waters in the generation of the molecular surface makes the volume occupied by those waters unavailable for penetration by mobile ions. Also, as we are using a dielectric constant of 2 for the interior domain of the molecular surface, the electrostatic potential and field are also affected. As predicted by O'Brien and White (1978), however, the interior dielectric constant is observed to have very little effect on electrophoretic mobility. Because of this, differences in μ arising from inclusion or exclusion of bound waters can be attributed to differences in ion accessible surfaces. Fig. 7 is very similar to Fig. 6 with $N = 128$ and $\sigma = 0.30$ nm. However, the 101 waters have been left out of the calculation of both the Stern and the molecular surfaces. Somewhat larger values of σ_s 0.46 and 0.52 nm) are required for values of D_t of 11.1×10^{-7} and 10.6×10^{-7} cm^2/s in this case. Leaving the 101 waters out of the molecular surface, but including them in the Stern surface (same values of σ_s as in Fig. 6) give results nearly identical to those of Fig. 7. The important difference between the models used in Figs. 6 and 7 is the larger volume of the Stern layer in the latter case and the larger magnitude of the net counterion charge within this volume. This explains the lower mobilities seen in Fig. 7. Leaving out the 101 crystallographic waters yields mobilities in better agreement with experiment at low pH, but this does not work so well at higher pH. In the remainder of this work, the 101 crystallographic waters will be included in generating the molecular and the Stern surfaces. Including a Stern layer of 0.15 nm in the Henry model (linear PB) reduces the calculated mobilities by 15% and also brings the mobilities of that simple model into better agreement with experiment. However, the Henry model by itself cannot assess the importance of polyion shape and charge distribution on mobility.

Other factors that also may affect μ in the BE modeling procedure are the number of surfaces used to generate the molecular and the Stern surfaces, N, as well as the orientation of the "starting octahedron" relative to the crystal structure coordinates. The diamonds in Fig. 8 correspond to the diamonds in Fig. 6 ($N = 128$, $\sigma = 0.30$ nm, $\sigma_s = 0.39$ nm), and the squares to experimental mobilities. The crosses correspond to $N = 512$, $\sigma = 0.30$ nm, and $\sigma_s = 0.37$ nm. A choice of $\sigma_s = 0.37$ yields $D_t(20°C) = 11.1 \times 10^{-7}$ cm^2/s. Increasing the number of surfaces from 128 to 512 results in a small reduction in mobility. In the limit of large N, the mobility is expected to become independent of N, and that limit has almost been reached by $N = 128$. Another criterion that can be used to assess how accurately the triangulated surface conforms to the actual "surface" of the structure is to rotate the starting octahedron, thereby generating an entirely different triangulated surface. For sufficiently large N, the mobility should become independent of the orientation of the starting octahedron. The triangles in Fig. 8 are for a model very similar to that shown by the crosses; except that the starting octahedron has first been rotated 45° about the z axis and then by 45° about the intermediate y axis. As expected, μ for both the rotated and nonrotated starting structures is in good agreement. In a related study, the interior dielectric constant was taken to be 20 instead of 2, but other conditions were identical to those of the crosses in Fig. 8. The calculated mobilities are slightly lower than the crosses in Fig. 8 and to a good approximation are coincident with the triangles. Evidently, the interior dielectric constant has only a small effect on electrophoretic mobility.

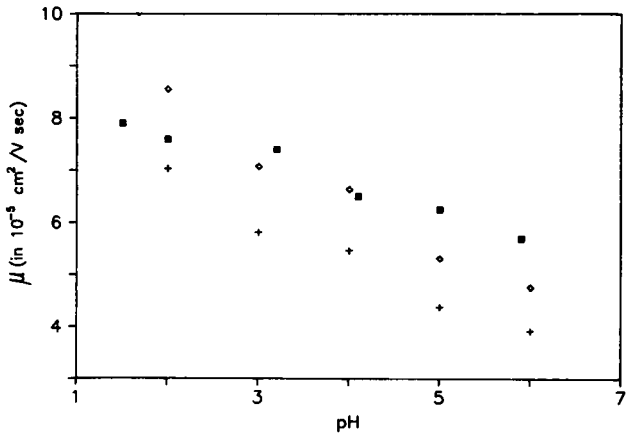

FIGURE 7 Experimental and BE mobilities (Stern layer included). Similar to Fig. 6, except that the 101 crystallographic waters have not been included in generating the molecular surfaces.

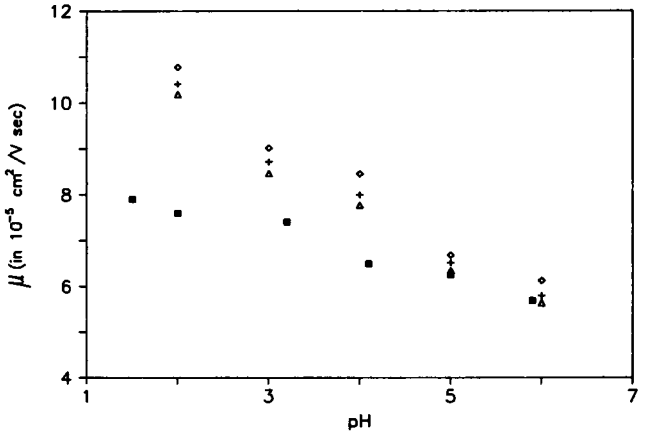

FIGURE 8 Experimental and BE mobilities ($N = 128$ and $N = 512$). ■, Experimental mobilities by squares. All BE studies have $\sigma = 0.30$ nm and σ_s chosen to yield $D_t(20°C) = 11.1 \times 10^{-7}$ cm^2/s. ◇ and + correspond to $N = 128$ and $N = 512$, respectively. ◇ also correspond to $N = 512$, except that the starting structure is different, as discussed in the text.

One feature of all the BE models considered so far is that they overestimate the dependence of mobility on pH. The problem is probably not due to inaccuracies in the charge state of lysozyme because the pK's of the residues are well known (Kuramitsu and Hamaguchi (1980). Even though the values of pK have largely been determined at 25°C and those of the μ at 0°C, the ionization enthalpies of Asp 52 and Glu 35 are nearly zero (Kuramitsu et al., 1977), so we expect pK to have only a small temperature dependence. Although a large dependence of pK on the salt concentration is expected, most pK determinations have been carried out at 0.10 molar monovalent salt, which is close to the 0.15 M salt employed in the mobility studies considered in this work. A factor that could account for the weaker than expected dependence of mobility on pH is a pH-dependent D_t (or σ_s). As Figs. 5 and 6 show, a small difference in D_t can translate into large differences in μ. Inasmuch as the net charge on lysozyme increases as pH decreases and water mobility is reduced more in the vicinity of a charged residue than a polar one (Brooks and Karplus, 1989), reducing the pH of lysozyme could be accompanied by a slight increase in effective σ_s (or a decrease in D_t). Shown in Fig. 9, superimposed on the experimental mobilities (squares), are BE mobilities for different σ_s. The curves from top to bottom correspond to $\sigma_s = 0.37$ (solid curve), 0.395, 0.42 (dotted curve), 0.45, and 0.48 nm. In the BE models, $N = 512$, $\epsilon_i = 2$, $\sigma = 0.30$ nm, and the starting structure is unrotated. The values of $D_t(20°C)$ that correspond to these values of σ_s are 11.06×10^{-7}, 10.84×10^{-7}, 10.66×10^{-7}, and 10.23×10^{-7} cm^2/s, respectively. A σ_s of 0.48 nm reproduces μ at pH = 2, but a lower value, in the range 0.42–0.45 nm is most consistent in the pH range of 3–4. Near a pH of 5 and 6, a σ_s of 0.38 nm appears appropriate. In summary, a small decrease in D_t with increasing pH could account for the dependence of μ on pH. A systematic study of D_t versus pH for hen egg lysozyme, which, to the best of our knowledge has not been carried out, would be of considerable value in addressing this issue.

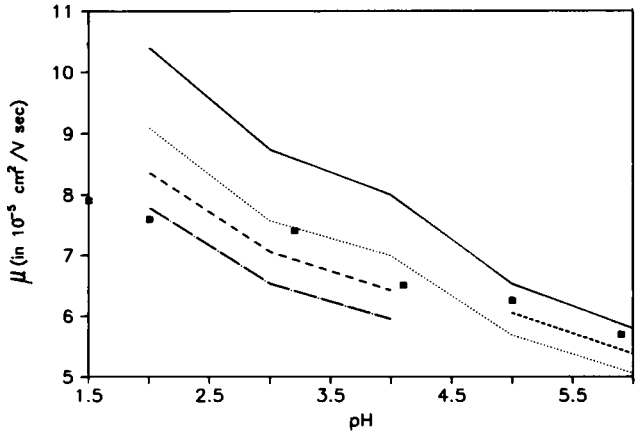

FIGURE 9 Effect of σ, on μ. Experimental mobilities (■) and BE mobilities ($N = 512$, $\sigma = 0.30$ nm, curves). From top to bottom: solid curve, $\sigma_s = 0.37$ nm; short-dashed curve, $\sigma_s = 0.395$ nm; dotted curve, $\sigma_s = 0.42$ nm; long-dashed curve, $\sigma_s = 0.45$ nm; dashed–dotted curve, $\sigma_s = 0.48$ nm.

SUMMARY

In this work, a numerical algorithm has been developed to calculate the electrophoretic mobility of rigid model polyions in the absence of ion relaxation. The polyion is treated as a low dielectric volume element of arbitrary shape and charge distribution and the surrounding solvent as a dielectric and hydrodynamic continuum. Boundary element methods are used to solve the linearized Poisson–Boltzmann and Navier–Stokes equations. The electrophoretic mobility is obtained from the total electrostatic and hydrodynamic forces on a translating polyion in a constant external electric field. We have tested the algorithm by applying it to spherical polyions with different charge distributions. It is then applied to detailed models of lysozyme derived from the crystal structure of the enzyme.

The electrophoretic mobility is sensitive to the properties of the solvent and ion distribution in the immediate vicinity of the polyion surface. In the modeling studies carried out here, this is reflected in the sensitivity of the calculated mobilities with the definition of the Stern layer, as demonstrated in Fig. 4–6. Although the inclusion of a Stern layer in the model is a simplification of the actual problem, it does account in an approximate way for the limited mobility of solvent and ions near the polyion surface. It would be straightforward to treat more complex models such as the use of different Stern exclusion radii for charged, polar, and apolar residues. However, given the assumptions already inherent in the model, such refinements seem unwarranted at this time. In comparing Figs. 6 and 7, it is also evident that the distribution of solvent ions within the Stern layer influences the electrophoretic mobility in a significant way. Further refinements in modeling the electrophoresis should address not only questions concerning the solvent near the polyion surface but the distribution of the solvent ions as well. These refinements are beyond the scope of the present work. For the present, we can simply say that the present model yields mobilities in fair agreement with experiment for reasonable choices of the molecular and Stern surfaces. However, this agreement is only qualitative because of model limitations. As discussed at the end of the last section, the stronger than expected dependence of mobility with pH can possibly be attributed to a pH-dependent translational diffusion constant. Finally, mobilities are found to be fairly insensitive to the choice of the interior dielectric constant as predicted by O'Brien and White (1978). It is hoped that this work will stimulate further experimental and theoretical studies of free solution electrophoresis of macromolecules.

REFERENCES

Allison, S. A., and P. Nambi. 1992. Transport of charged macromolecules in an electric field by a numerical method. 1. Application to a sphere. *Macromolecules.* 25:3971–3978.

Allison, S. A., and P. Nambi. 1994. Electrophoresis of spheres by a discretized integral equation/finite difference approach. *Macromolecules.* 27:1413–1422.

Beychok, S., and R. C. Warner. 1959. Denaturation and electrophoretic behavior of lysozyme. *J. Am. Chem. Soc.* 81:1892–1897.

Booth, F. 1950. The Cataphoresis of spherical, solid non-conducting particles in a symmetrical electrolyte. *Proc. R. Soc. London Ser.* A. 203: 514–533.

Brenner, H. 1963. The Stokes resistance of an arbitrary particle. *Chem. Eng. Sci.* 18:1–25.

Brooks, C. L., and M. Karplus. 1989. Solvent effects on protein motion and protein effects on solvent motion. *J. Mol. Biol.* 208:159–181.

Brune, D., and S. Kim. 1993. Predicting protein diffusion coefficients. *Proc. Natl. Acad. Sci. USA.* 90:3835–3839.

Dubin, S. B., J. H. Lunacek, and G. B. Benedek. 1967. Observation of the spectrum of light scattered by solutions of biological macromolecules. *Proc. Natl. Acad. Sci. USA.* 57:1164–1171.

Dubin, S. B., N. A. Clark, and G. B. Benedek. 1971. Measurement of rotational diffusion coefficient of lysozyme by depolarized light scattering: configuration of lysozyme in solution. *J. Chem. Phys.* 54:5158–5164.

Garcia de la Torre, J., and V. A. Bloomfield. 1981. Hydrodynamic properties of complex, rigid, biological macromolecules: theory and applications. *Q. Rev. Biophys.* 14:81–139.

Grossman, P. D. 1992. Free solution capillary electrophoresis. In Capillary Electrophoresis: Theory and Practice. P. D. Grossman and J. C. Colburn, editors. Academic Press, San Diego, CA. Chapter 4.

Henry, D. C. 1931. The cataphoresis of suspended particles. Part I. The equation of cataphoresis. Proc. R. Soc. London Ser. A. 133:106–129.

Holmes, D. L., and N. C. Stellwagen. 1991. Estimation of polyacrylamide gel pore size from Ferguson plots of normal and anomolously migrating DNA fragments. *Electrophoresis.* 12:253–263.

Hückel, E. 1924. The cataphoresis of the sphere. Phys. Z. 25:204–210.

Hunter, R. J. 1987. Transport properties of suspensions. *In* Foundations of Colloid Science. Vol. 1. Oxford University Press, Oxford, UK. Chapter 9.

Juffer, A. H., E. F. F. Botta, B. A. M. Van Keulen, A. Van Der Ploeg, and H. J. C. Berendsen. 1991. The electric potential of a macromolecule in a solvent: a fundamental approach. *J. Comp. Phys.* 97:144–171.

Kim, S., and S. J. Karrila. 1991. Microhydrodynamics. Principles and Selected Applications. Butterworth-Heinemann, Stoneham, MA.

Kuntz, I. D., and W. Kauzmann. 1974. Hydration of proteins and polypeptides. *Adv. Prot. Chem.* 28:239–345.

Kuramitsu, S., and K. Hamaguchi. 1980. Analysis of the acid-base titration curve of hen lysozyme. *J. Biochem. (Tokyo).* 87:1215–1219.

Kuramitsu, S., K. Ikeda, and K. Hamaguchi. 1977. Effects of ionic strength and temperature on the ionization of the catalytic groups, Asp 52 and Glu 35, in hen lysozyme. *J. Biochem. (Tokyo).* 82:585–597.

Ladyzhenskaya, O. A. 1963. The Mathematical Theory of Viscous Incompressible Flow. Gordon & Breach, New York.

Levitt, M., and R. Sharon. 1988. Accurate simulation of protein dynamics in solution. *Proc. Natl. Acad. Sci. USA.* 85:7557–7561.

O'Brien, R. W., and L. R. White. 1978. Electrophoretic mobility of a spherical colloidal particle. *J. Chem. Soc. Faraday Trans. 2.* 74:1607–1626.

Overbeek, J. Th. G. 1950. Quantitative interpretation of the electrophoretic velocity of colloids. *In* Advances in Colloid Science, Vol. III. H. Mark, editor, Interscience Publishing, New York.

Pakdel, P., and S. Kim. 1991. Mobility and stresslet functions of particles with rough surfaces in viscous fluids: a numerical study. *J. Rheol.* 35: 797–823.

Rupley, J. A., and G. Careri. 1991. Protein hydration and function. *Adv. Prot. Chem.* 41:37–172.

Schellman, J. A., and D. Stigter. 1977. Electrical double layer, zeta potential, and electrophoretic charge of double-stranded DNA. *Biopolymers.* 16: 1415–1434.

Shaw, D. J. 1980. Introduction to Colloid and Surface Chemistry, 3rd ed. Butterworth, London.

Smoluchowski, M. 1921. Electro-osmosis and current flow. *In* Handbuch der Electrizitat und des Magmetismus, Vol. II. L. Graetz, editor. Barth, Leipzig.

Sophianopoulos, A. J., and K. E. Van Holde. 1964. Physical studies of muramidase (lysozyme). *J. Biol. Chem.* 239:2516–2524.

Squire, P. G., and M. E. Himmel. 1979. Hydrodynamics and protein hydration. *Arch. Biochem. Biophys.* 196:165–177.

Stigter, D. 1978. Electrophoresis of highly charged colloidal cylinders in univalent salt solutions. 1. Mobility in transverse field. 2. Random orientation in external field and application to polyelectrolytes. *J. Phys. Chem.* 82:1417–1423, 1424–1429.

Teller, D. C., E. Swanson, and C. De Haen. 1979. The translational friction coefficient of proteins. *Methods Enzymol.* 61:103–124.

Teubner, M. 1982. The motion of charged colloidal particles in electric fields. *J. Chem. Phys.* 76:5564–5573.

Venable, R. M., and R. W. Pastor. 1988. Frictional models for stochastic simulations of proteins. *Biopolymers.* 27:1001–1014.

Wiersema, P. H., A. L. Loeb, and J. Th. G. Overbeek. 1966. Calculation of the electrophoretic mobility of a spherical colloid particle. *J. Colloid Interface Sci.* 22:78–99.

Yoon, B. J. 1991. Electrophoretic motion of spherical particles with a nonuniform charge distribution. *J. Colloid Interface Sci.* 142:575–581.

Yoon, B. J., and S. Kim. 1989. Electrophoresis of spheroidal particles. *J. Colloid Interface Sci.* 128:275–288.

Yoon, B. J., and A. M. Lenhoff. 1990. A boundary element method for molecular electrostatics with electrolyte effects. *J. Comp. Chem.* 11:1080–1086.

Youngren, G. K., and A. Acrivos. 1975. Stokes flow past a particle of arbitrary shape: a numerical method of solution. *J. Fluid Mech.* 69: 377–403.

Zhou, H.-X. 1993. Boundary element solution of macromolecular electrostatics: interaction energy between two proteins. *Biophys. J.* 65:955–963.